A Flexible Loop at the Dimer Interface is a Part of the Active Site of the Adjacent Monomer of *Escherichia coli* Orotate Phosphoribosyltransferase[†,‡]

Anette Henriksen,[*,§] Nushin Aghajari,[§] Kaj Frank Jensen,[||] and Michael Gajhede[§]

Center for Crystallographic Studies, University of Copenhagen, Universitetsparken 5, DK-2100 København Ø, Denmark, and Center for Enzyme Research, University of Copenhagen, Sølvgade 83 H, DK-1307 København K, Denmark

Received September 18, 1995; Revised Manuscript Received January 15, 1996[⊗]

ABSTRACT: Orotate phosphoribosyltransferase (OPRTase) is involved in the biosynthesis of pyrimidine nucleotides. α-D-ribosyldiphosphate 5-phosphate (PRPP) and orotate are utilized to form pyrophosphate and orotidine 5′-monophosphate (OMP) in the presence of divalent cations, preferably Mg^{2+}. OMP is thereafter converted to uridine 5′-monophosphate by OMP decarboxylase. We have determined the 2.4 Å structure of *Escherichia coli* OPRTase, ligated with sulfate, by molecular replacement and refined the structure to an *R*-factor of 18.3% for all data. In the structure of the *E. coli* enzyme we have determined the fold of a flexible loop region with a highly conserved amino acid sequence among OPRTases, a region known to take part in catalysis. The structure of this region was not determined in the model used for molecular replacement, and it involves interactions at the dimer interface through a bound sulfate ion. Crystalline *E. coli* OPRTase is a homodimer, with sulfate ions inhibiting enzyme activity bound in the dimer interface close to the flexible loop region. Although this loop is very close in space to the sulfate binding site, and sulfate is found in both interfaces of the homodimer, the loop structure is only traceable in one monomer. We expect that the mobility of this loop is important for catalysis, and, on the basis of the reported structure and the structure of *Salmonella typhimurium* OPRTase·OMP, we propose that the movement of this loop in association with the movement of OMP is vital to catalysis. Apart from the flexible loop region and a solvent-exposed loop (residues 158−164), the most significant differences in structure between *S. typhimurium* OPRTase·OMP and *E. coli* OPRTase are found in the substrate binding regions: the 5′-phosphate binding region (residues 120−131), the binding region for the orotate part of OMP (residues 25−27), and the pyrophosphate binding region (residues 71−73).

Orotate phosphoribosyltransferase (OPRTase) provides the pathway for *de novo* biosynthesis of pyrimidine nucleotides by catalyzing the Mg^{2+} dependent formation of orotidine 5′-monophosphate (OMP), the pyrimidine nucleotide from which uridine 5′-monophosphate is synthesized (Figure 1) (Musick, 1981). Other phosporibosyltransferases (PRTases) are involved in synthesis or salvage of purine and pyrimidine nucleotides and also in the synthesis of the aromatic amino acids histidine and tryptophan and the pyridine coenzymes NAD and NADP (Musick, 1981, Jensen, 1983). The PRTases all transfer a ribosyl phosphate group from α-D-ribosyldiphosphate 5-phosphate (PRPP) with the C1′ of ribose as the target position. A motif of 12 amino acid residues also found in PRPP synthetases has been proposed to represent a common PRPP binding motif (Hershey & Taylor, 1986; Hove-Jensen et al., 1986). This short sequence is the only well-conserved sequence observed in the group of PRTases and structurally it represents a strand−loop−helix structure.

In two of the known three-dimensional structures of PRTases, OPRTase·OMP (Scapin et al., 1994) and hypoxanthine-guanine-PRTase(HGPRTase)·GMP (Eads et al., 1994), a homologous stretch of amino acid residues showed very poor density. This loop was left structurally non-determined in OPRTase, while a tentative fitting of the sequence to the electron density was made in one HGPRTase monomer, showing a loop extending into the solvent. The sequence of this very flexible loop is highly conserved among OPRTases, and residues from the loop are important for catalysis (Grubmeyer et al., 1993; Ozturk et al., 1995a,b). The third published PRTase structure, glutamine-PRPP-amidotransferase·AMP (amido-PRTase) belongs to the glutamine amidotransferase enzyme family as well (Smith et al., 1994). This enzyme has an even longer extended structure in a similar position, making contacts between neighboring subunits. In amido-PRTase the region has been proposed to be involved in feedback regulation of enzyme activity (Smith et al., 1994).

The reaction mechanism of OPRTases is still a subject of discussion. The transferase reaction proceeds with inversion at the anomeric carbon, and an oxocarbonium-like transition state has been proposed (Bhatia et al., 1990; Goitein et al., 1978) as well as an S_N1-like mechanism (Goitein et al., 1978). We have initiated structural investigations of *E. coli* OPRTase to establish the structural basis for the PRTase function in this quite small non-allosterically controlled enzyme.

[†] This work was funded by the Danish National Research Foundation.

[‡] Coordinates for this structure have been deposited in the Brookhaven Protein Data Bank. The access code is 1oro.

* Author to whom correspondence should be addressed.

[§] Center for Crystallographic studies.

[||] Center for Enzyme Research.

[⊗] Abstract published in *Advance ACS Abstracts,* February 15, 1996.

[1] Abbreviations: OPRTase, orotate phosphoribosyltransferase; OMP, orotidine 5′-monophosphate; PRPP, α-D-ribosyldiphosphate 5-phosphate; AMP, adenosine 5′-monophosphate; GMP, guanosine 5′-monophosphate; PRTase, phosphoribosyltransferase; HPRTase, hypoxanthine−guanine phosphoribosyltransferase; amido-PRTase, glutamine PRPP amidotransferase; F_o, measured structure factor amplitude; F_c, calculated structure factor amplitude; $(F_o - F_c)\alpha_{calc}$, electron density calculated with $(|F_o|-|F_c|)$ coefficients and phases calculated from the coordinates; $(2F_o-F_c)\alpha_{calc}$, electron density calculated with $(2|F_o|-|F_c|)$ coefficients and phases calculated from the coordinates; R_{cryst}, $\Sigma||F_o|-|F_c||/\Sigma|F_o|$; R_{merge}, $\Sigma\Sigma\langle I\rangle - I/\Sigma\Sigma I$.

0006-2960/96/0435-3803$12.00/0

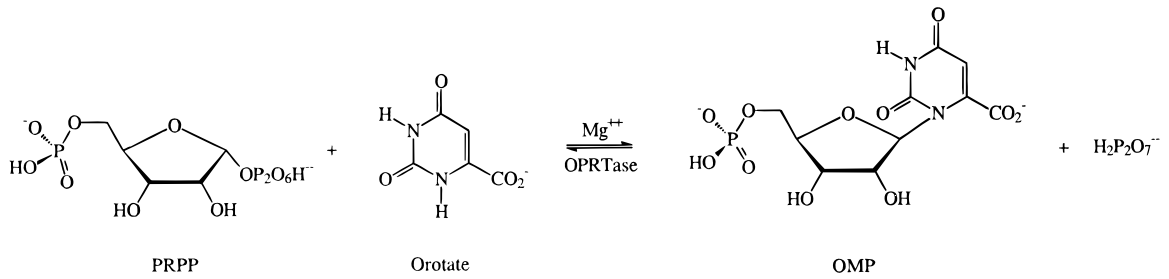

FIGURE 1: OMP formation as catalyzed by OPRTase.

E. coli OPRTase has been sequenced (Poulsen et al., 1983), overexpressed in *E. coli*, and purified to homogeneity (Jensen et al., 1992; Aghajari et al., 1994). Crystallization of the enzyme has been reported (Aghajari et al., 1994). Its kinetics are expected to be similar to the kinetics of *S. typhimurium* OPRTase (Bhatia et al., 1990), which is 97% identical to *E. coli* OPRTase.

We report the three-dimensional structure of *E. coli* OPRTase in its sulfate ligated form, solved and refined using diffraction data to a resolution of 2.4 Å. The crystal structure of *E. coli* OPRTase was determined by the molecular replacement program AMoRe (Navaza, 1994) with the monomer of *S. typhimurium* OPRTase·OMP (Scapin et al., 1994) as the search model.

EXPERIMENTAL PROCEDURES

Crystallization. Crystals of *E. coli* OPRTase were grown by the hanging drop vapor diffusion method as previously described (Aghajari et al., 1994). The crystals used in this study were grown against a reservoir of 2.1 M Na_2SO_4, 0.3 M citrate buffer, pH 4.8, at room temperature. No OPRTase substrates were added to the protein prior to crystallization. The crystals are orthorhombic, with space group $P2_12_12_1$ and the unit cell parameters $a = 54.9$ Å, $b = 71.1$ Å and $c = 104.2$ Å. There are two monomers per asymmetric unit each of 213 amino acid residues, related by a non-crystallographic 2-fold axis parallel to the crystallographic *b*-axis. This relationship between monomers produces a peak in the native Patterson function of 18 σ at the position (0.00, 0.50, 0.18). On the basis of the peak of the Patterson function, the true space group could also have been $P2_122_1$, with a pseudo 2-fold screw axis along the *b*-axis. This possibility was ruled out by the molecular replacement search, which gave no significant solutions for the latter space group.

The solvent content of the crystals is approximately 43%. They are X-ray sensitive, with a decay of intensities of about 50% over a one-day period, and they diffract to a resolution of 2.4 Å.

Data Collection and Processing. Data were collected from a single crystal on a Rigaku R-axis IIC image plate system, with a Rigaku RU200 rotating anode operated at 50 kV and 180 mA. The system was equipped with a graphite monochromator and a 0.5 mm collimator. The crystal to detector distance was 105 mm, and the exposure time per frame was 45 min; 39 frames of 2.0° oscillations were collected. The scale factor for the last frame was 2.5, and the *B*-factor for the same frame was −1.1. Integration of intensities was performed with the program Denzo (Otwinowski, 1993), while data averaging and reduction were done with programs from the CCP4 program package (Collaborative Computer Project, Number 4, 1994). An overview of the data quality is given in Table 1.

Table 1: Quality of the *E. coli* OPRTase Data in the Resolution Range 37−2.4 Å[a]

resolution (Å)	R_{fac}	R_{cum}	$I/\sigma I$	N_{meas}	N_{ref}	% possible
7.44	0.029	0.029	15.9	1574	500	86.7
5.33	0.047	0.036	12.0	2824	877	91.5
4.36	0.050	0.043	9.1	3625	1145	94.1
3.78	0.057	0.047	11.1	4140	1330	95.2
3.39	0.075	0.051	9.0	4531	1548	96.5
3.09	0.096	0.056	7.0	4785	1730	98.1
2.87	0.138	0.060	5.1	4915	1868	97.8
2.68	0.195	0.064	3.6	5116	2004	97.7
2.53	0.283	0.069	2.4	5367	2127	97.7
2.40	0.330	0.075	2.0	5672	2223	96.5
total		0.075	7.5	42549	15352	96.2

[a] R_{fac} is the *R*-factor on intensities in the resolution shell concerned. R_{cum} is the cumulated *R*-factor on intensities, N_{meas} is the number of measured reflections, and N_{ref} is the number of unique reflections.

Structure Determination. The crystal structure of *E. coli* OPRTase was solved by molecular replacement using the structure of *S. typhimurium* OPRTase·OMP (Scapin et al., 1994) without bound OMP as a model. The two structures have an amino acid sequence identity of 97%. Molecular replacement was done with the program AMoRe (Navaza, 1994), implemented in the CCP4 program package (Collaborative Computer Project, Number 4, 1994), and the molecular replacement search was carried out using only one monomer of the homodimer. The highest molecular replacement solution after rigid body refinement of the 25 highest translational solutions in space group $P2_12_12_1$ was significantly better than the rest, with an R_{cryst} of 52.1% to a resolution of 3 Å. A rotation and translation search was carried out using 10−4 Å data, while data between 10 and 3 Å was used in the rigid-body refinement. There was no spatial overlap between the molecules in the final molecular replacement solution.

The two molecules of the asymmetric unit formed the homodimer of OPRTase and differed from the homodimer of OPRTase·OMP of *S. typhimurium* by having the monomers related by a non-crystallographic 2-fold axis instead of a perfect crystallographic 2-fold axis. Inspection of the $(2F_o - F_c)\alpha_{calc}$ and $(F_o - F_c)\alpha_{calc}$ electron density map after rigid-body refinement confirmed the molecular replacement solution by showing density in one of the monomers for the flexible 103−107 loop, which is not present in the search model, and for the side chains differing from *S. typhimurium* OPRTase side chains in both monomers.

Structure Refinement. The model was manually fitted to the $(2F_o - F_c)\alpha_{calc}$ and the $(F_o - F_c)\alpha_{calc}$ maps after rigid-body minimization using computer graphics (O; Jones et al., 1991) and refined by energy minimization and molecular dynamics with the slow cool simulated annealing procedure of X-PLOR (Brünger, 1992; Brünger et al., 1987). Non-crystallographic symmetry restraints were applied in all refinement steps, keeping most of the β-strands and α-helices

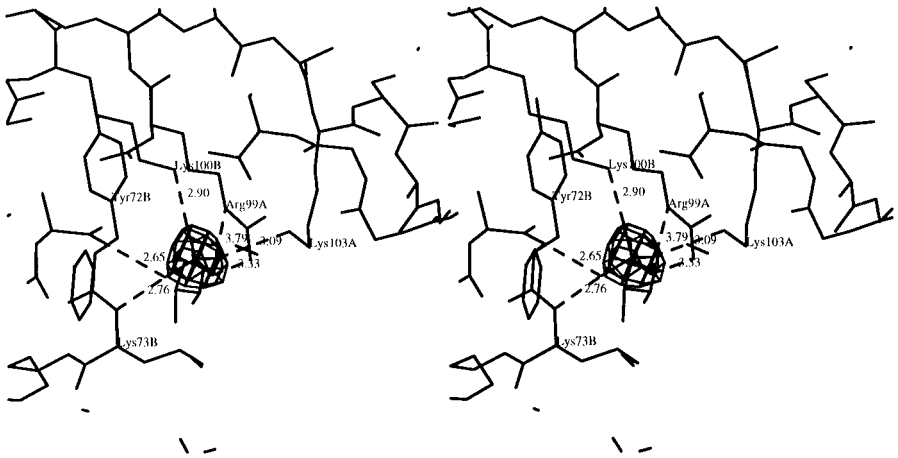

FIGURE 2: Stereodiagram of the OPRTase·SO_4^{2-} complex. The electron density is $(F_o - F_c)\alpha_{calc}$ at a level of 5σ, calculated without including SO_4^{2-} in the model. Hydrogen bond donors and hydrogen bond distances are shown.

backbone and side chain atoms restrained, which was justified by an improvement of the free *R*-value (Brünger, 1992) of 2%. Individual *B*-factors were refined but were restrained to be correlated to the *B*-factors of neighboring atoms. The structure was refined against 6.0−2.4 Å data, omitting a solvent mask, as no satisfactory model for the solvent mask was achieved, judged by the variation in the *R*-value. Following this refinement procedure the free R_{cryst}, based on a randomly selected 10% of the diffraction data, had fallen to 26.3% for 6−2.4 Å data. All data in this resolution range were included in subsequent refinement steps.

The initial free R_{cryst} was 39.7%, and solvent molecules were included in the model after structural refinement had reached a free R_{cryst} of 30%. Two sulfate ions were included, which could be identified from large and nicely resolved peaks (nine times the rms of the map) in the $(F_o - F_c)\alpha_{calc}$ map, at a distance of 4.2 Å from Arg99A N_ϵ and Arg99B N_ϵ (Figure 2). A level of three times the standard deviation in the $(F_o - F_c)\alpha_{calc}$ electron density map was chosen as a criterion for assignment of water molecules. No water molecules with *B*-factors larger than 50 Å^2 were accepted, and no additional water or sulfate molecules were included in the model after the inclusion of all data in the refinement.

Sulfate and Phosphate Inhibition of the OPRTase Reaction. To determine the implications of the binding of sulfate to the OPRTase dimer interface, inhibition studies were carried out to describe the effects of salts on OPRTase activity.

Spectrophotometric assays of OPRTase activity were carried out as described by Poulsen et al. (1983). The reactions (a total volume of 1 mL containing 100 mM Tris-HCl, pH 8.8, 6 mM $MgCl_2$, 2.5 mM orotate, 0.5 mM PRPP, and various concentrations of salts) were carried out at 37 °C. The reactions were initiated by addition of enzyme to the prewarmed mixture of the other components and monitored by measuring the decrease in absorbtion of UV light at 295 nm.

RESULTS AND DISCUSSION

The functional unit of *E. coli* OPRTase has been established to be a homodimer in solution (Poulsen et al., 1983) as have the OPRTase of *S. typhimurium* (Bhatia et al., 1990) and the human HGPRTase [which exist as a tetramer as well, depending on the ionic strength (Johnson et al., 1979; Strauss et al., 1978)]. The latter two enzymes also appeared as

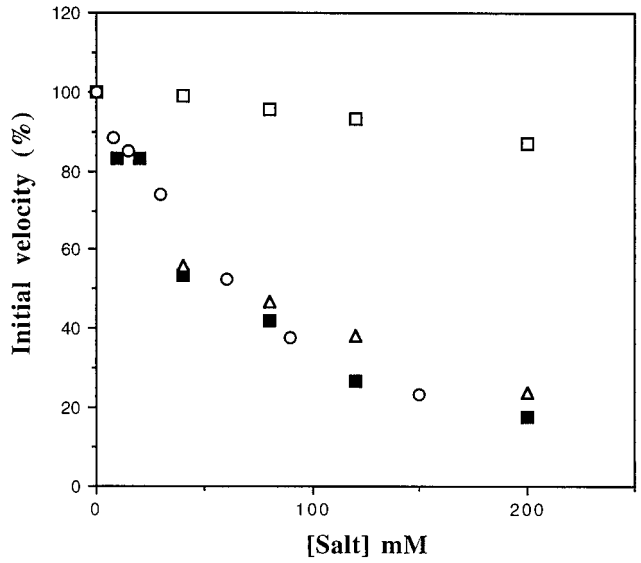

FIGURE 3: Effect of sulfate and phosphate upon the OPRTase catalysed conversion of PRPP to OMP: (□) NaCl, (○) K_2HPO_4, (■) $(NH_4)_2SO_4$, (△) Na_2SO_4.

homodimers in their crystal forms co-crystallized with OMP (Scapin et al., 1994) and GMP (Eads et al., 1994), respectively. The two monomers of *S. typhimurium* OPRTase·OMP were additionally related by a crystallographic 2-fold axis, giving crystals with only one molecule in the asymmetric unit. This is not the case for the sulfate-ligated form of *E. coli* OPRTase. Here the two monomers are related by a non-crystallographic 2-fold axis, as observed for HPRTase·GMP (Eads et al., 1994). In the crystal structure, the amino acid residues for the two molecules are labeled 1A−213A and 1B−213B.

Inhibition. We found that Na_2SO_4, $(NH_4)_2SO_4$, and K_2HPO_4 inhibited the OPRTase reaction to about equal extent, i.e., 40−50 mM of these anions gave 50% inhibition, while NaCl (0.2 M) caused little or no inhibition (Figure 3).

Structural Quality. The current model includes 3273 non-hydrogen protein atoms out of 3322 (the loop 102B−108B is not included in the final structure), two sulfate ions, and 118 additional solvent molecules. The conventional R_{cryst} for the structure is 18.3% using all data in the 6−2.4 Å range and 21.7% for all data in the 30−2.4 range. The rms deviations from ideal geometry and refinement statistics are listed in Table 2.

Table 2: Refinement Statistics for *E. coli* OPRTase

Parameters		
no. of non-hydrogen protein atoms	3273	
no. of solvent molecules	118	
no. of sulfate molecules	2	
B-factor model	restrained	isotropic
Diffraction Agreement		
resolution (Å)	30−2.4	6−2.4
no. of reflections	15350	14383
σ cutoff	0	0
R_{crys} (%)	21.7	18.3
Stereochemical Ideality		
rmsd bond lengths (Å)		0.006
rmsd bond angles (deg)		1.46
rmsd impropers (deg)		1.06
rmsd dihedrals (deg)		21.17
average *B* (Å^2)		23.4

A Ramachandran plot calculated with the program PROCHECK (Laskowski et al., 1993) shows no non-glycine residues in disallowed regions. The Ala71A−Tyr72A and Ala71B−Tyr72B peptide bonds were fitted as cis-peptides to achieve a good fit to the electron density map. After the peptide bonds were flipped, the structure could be refined nicely in these areas, the backbone nitrogens of residues 72 and 73 serving as hydrogen donors for the bound sulfate groups.

The average *B*-factor for all protein atoms is 23.4 Å^2. Apart from the flexible loop in one monomer (102B−108B), a break in the backbone 1σ ($2F_o - F_c$)α_{calc} density also occurs in the loops: 26A−27A and 26B−27B. These residues are known to take part in OMP binding (Scapin et al., 1994) and are very flexible when OMP is not present. Another quite flexible region is the 156−164 loop between strand B6 and helix A5. This loop is solvent exposed but has an unbroken 1σ ($2F_o - F_c$)α_{calc} density. A real-space fit for the protein calculated with the program O (Jones et al., 1986) shows a good fit between electron density and model for all other areas.

A weak level of ($F_o - F_c$)α_{calc} electron density was visible protruding into the solvent around the 102B−108B flexible loop. It was, however, not possible to refine this part of the structure, and it has been left out of the final model.

Description of the Structure. The monomer of *E. coli* OPRTase contains 213 amino acid residues and is composed of ten β-strands (labeled B1−B7) and seven α-helices (labeled A1−A7). A ribbon diagram of the structure is shown in Figure 4a,b, while a full description of secondary structure elements is given in Table 3. Apart from the seven regular α-helices a single turn of a 3_{10}-helix is found between strand B2 and helix A2: residues 37A−40A and residues 37B−40B.

The structure of *E. coli* OPRTase closely resembles the structure of *S. typhimurium* OPRTase·OMP (Scapin et al., 1994) with a rms difference between the molecules of 0.682 Å for C_α-atoms (Figure 5). The areas of greatest divergence are the 5′-phosphate binding region called the PRPP binding motif, the sulfate binding region, the region binding the orotate moiety of OMP in the *S. typhimurium* structure, and a solvent-exposed loop (residues 58−64). Consequently, the topology of the *E. coli* and the *S. typhimurium* enzymes is similar. However, not all β-strands of the *E. coli* structure were assigned as β-strands in the OMP bound enzyme. Figure 4c is a schematic representation of the enzyme topology.

As the monomers of *E. coli* OPRTase are essentially identical (rms difference 0.482 Å for all protein atoms except the flexible loop) only the 1A−213A monomer will be described in the following, except for regions with distinct differences.

The core structure of the enzyme resembles the core structure found in OPRTase·OMP, HGPRTase·GMP and amido-PRTase·AMP: a five-stranded parallel β-sheet surrounded by four α-helices (Figure 4a−c). This can be seen as a variation of the nucleotide binding fold (Schultz, 1992; Walker et al., 1982). The first half of the α/β-sheet (Richardson, 1981) of OPRTase contains the secondary structure elements A2, B3, A3, and B4. The crossover to the second half of the α/β-sheet consists of a loop (102−108), referred to as the flexible loop, and a short β-strand antiparallel to the core sheet. This antiparallel β-strand (B5′) has not been reported for the OMP-bound enzyme, probably due to a larger degree of flexibility in this region, as the flexible loop was not traceable in that structure.

In HGPRTase the crossover connection is a flexible loop and an α-helix, and in amido-PRTase the corresponding region is composed of two strands and a short α-helix forming a "flag" structure protruding from one monomer to the other. In *E. coli* OPRTase, the loop 102−108 was only traceable in one of the subunits (Figure 6) and makes interactions from one monomer to the active site of the adjacent monomer through a bound sulfate ion. In the other subunit the loop 102B−108B showed only weak density and seems to be protruding into the solvent with no interactions to the adjacent monomer.

The second half of the core structure is composed of B5, A4, B6, A5, and B7, with B5-loop-A4 contributing to the so called "PRPP binding motif" (^{120}VMLVDDVITAGT^{131}) (Hove-Jensen et al., 1986). The three PRTase structures all have the PRPP binding motif going out from the central β-strand of the core sheet, but the arrangement of the four α-helices is somewhat different in HGPRTase. Here the helix following the PRPP binding motif is the last helix of the α/β-sheet, while in the core topology of OPRTase and the PRPP binding domain of amido-PRTase, the helix with the same function is the second to last helix of the α/β-sheet. The structure of this helix is slightly different in the two monomers of *E. coli* OPRTase. In the 1A−213A monomer, the A4 helix starts as a 3_{10}-helix, the α-helix extending from 133A to 143A. In the second monomer the A4 helix starts as a true α-helix and extends from 130B to 143B. In amido-PRTase the backbone of this helix segment is involved in hydrogen bonds to the 5′-phosphate of AMP bound in the catalytic site. The difference in the fold of the PRPP binding motif between the two monomers of *E. coli* OPRTase reflects flexibility and may be related to the ability of these regions to adopt different conformations involved in the catalytic mechanism of the enzyme.

Above the core, as viewed in figure 4a, is a domain consisting of three α-helices and two β-strands. The amino-terminal part of the protein (1−41) forms the first α-helix and two bent antiparallel β-strands: B1, B1′ and B2, B2′. The Kabsch and Sander algorithm (1983) defines the extension of the β-strands to be 17−25 and 29−36, but Gly21 and Pro32 introduce bends in the strands. Gly21 and Pro32 are highly conserved among both OPRTases and UMP synthetases, indicating that these kinks are of structural importance. The carboxy-terminal part of the structure (184−213) forms two antiparallel α-helices lying perpendicular to the amino-terminal helix. The upper domain does not resemble structures in HGPRTase or amido-PRTase in

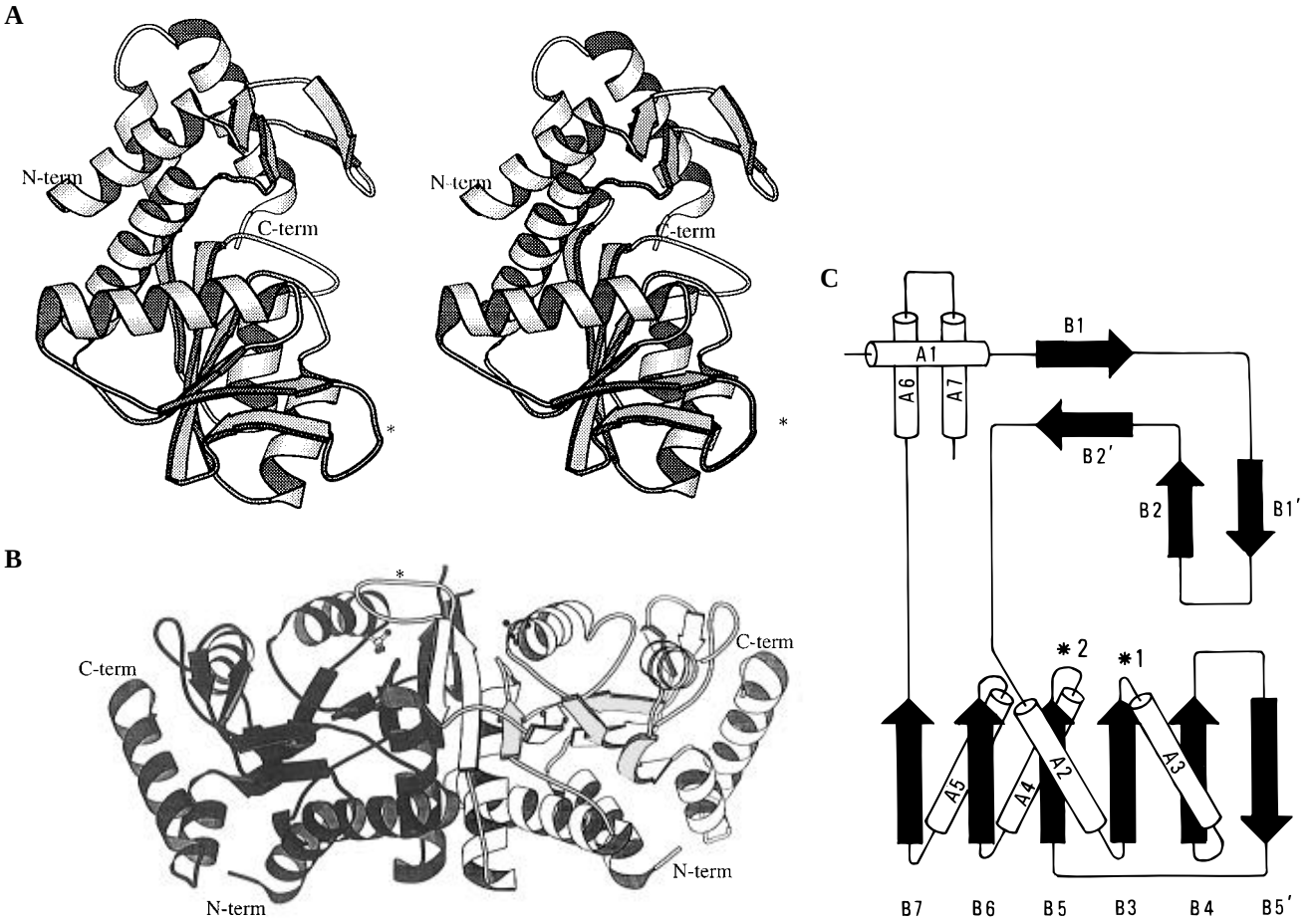

FIGURE 4: (a) Ribbon diagram of the three-dimensional structure of monomer 1−213 of *E. coli* OPRTase. An asterisk marks the flexible loop. (b) Ribbon diagram of the three-dimensional structure of *E. coli* OPRTase. Bound sulfates are shown as ball-and-stick models, and the flexible loop of one monomer (grey) covers the sulfate binding site in the other monomer (black). The flexible loop is marked by an asterisk. The non-crystallographic 2-fold axis between the two monomers can be observed in the vertical plane. The figures were generated with the program Molscript (Kraulis, 1991). For a complete description of secondary structure elements see Table 3. (c) Schematic representation of the topology of a monomer of OPRTase. The lower part of the figure represents the PRPP binding domain.*1 marks the sulfate binding loop, while *2 marks the 5′-phosphate binding loop.

Table 3: Secondary Structure Elements of *E. coli* OPRTase as Defined by the Kabsch and Sander Algorithm (1983) and Calculated by the Program PROCHECK (Laskowski *et al.*, 1993)

name (as in Figure 4c)	residues involved	secondary structure
A1	2A−15A, 2B−15B	α-helix
B1	17A−20A, 17B−20B	*β*-strand
B1′	22A−25A, 22B−25B	*β*-strand
B2	29A−31A, 29B−31B	*β*-strand
B2′	33A−36A, 33B−36B	*β*-strand
A2	42A−61A, 42B−61B	α-helix
B3	66A−69A, 66B−69B	*β*-strand
A3	73A−90A, 73B−90B	α-helix
B4	94A−99A, 94B−99B	*β*-strand
B5′	110A−114A, 110B−114B	*β*-strand
B5	118A−124A, 118B−124B	*β*-strand
A4	133A−143A, 130B−143B	α-helix
B6	146A−155A, 146B-155B	*β*-strand
A5	165A−175A, 165B−175B	α-helix
B7	177A−183A, 177B−183B	*β*-strand
A6	184A−192A, 184B−192B	α-helix
A7	197A−212A, 197B−212B	α-helix

any way and is associated with the base specificity of the enzyme. In the sulfate-ligated enzyme, the loop between B1 and B2 is quite disordered, indicated by high *B*-factors. This disorder is not as pronounced when OMP is bound to the enzyme in the OPRTase·OMP complex (Scapin et al., 1994). In this structure the carboxylate of the orotate moiety makes a hydrogen bond to the backbone nitrogen of Lys26 and the ribose O3′ forms a hydrogen bond to the N_ζ of the same Lys, thereby stabilizing the fold in an induced fit.

The Dimer Interface and the Active Site. The dimer interface consists of the regions Asn41−Arg51 (helix A2), Tyr72−Lys100 (helix A3−loop−strand B4), and Gly113−Ser114 (strand B5), and it involves a total of 25 amino acid residues from each monomer making direct interactions with the other monomer (the maximum distance for an interaction being defined as 3.9 Å). The flexible loop has no direct amino acid interactions at the dimer interface, but it folds over the active site and forms a bridge toward Lys26B of the adjacent monomer (Figure 7). However, N_ζ of Lys103A from the flexible loop forms a hydrogen bond to the bound inhibitory sulfate ion, which also is hydrogen bonded to the backbone nitrogen of Tyr72B (adjacent monomer), the backbone nitrogen of Lys73B (adjacent monomer), N_ζ of Lys100B (adjacent monomer), and N_ϵ of Arg99A (same monomer) (Figures 2 and 7). Lys73A and Lys73B can be refined in two different conformations: as hydrogen bonded to the inhibitory sulfate or as hydrogen bonded to the conserved PRTase residues Asp125A and Asp125B from the "PRPP-binding motif." The binding of the sulfate ion probably mimics the binding of pyrophosphate and the binding of the pyrophosphate moiety of PRPP to OPRTase, as the residues involved in hydrogen bonding to sulfate are among the residues described to be protected against chemi-

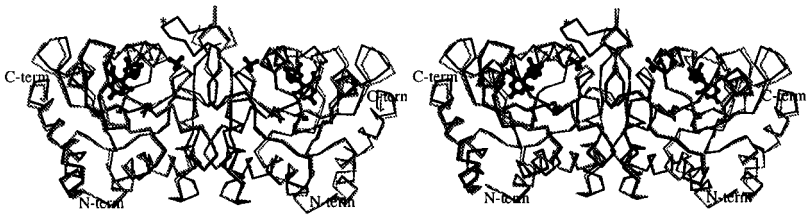

FIGURE 5: Stereodiagram of the α-carbon tracing of *E. coli* OPRTase (black lines) superimposed on the α-carbon tracing of the *S. typhimurium* OPRTase structure (grey lines). OMP and sulfate are shown as ball-and-stick models. An asterisk marks the flexible loop.

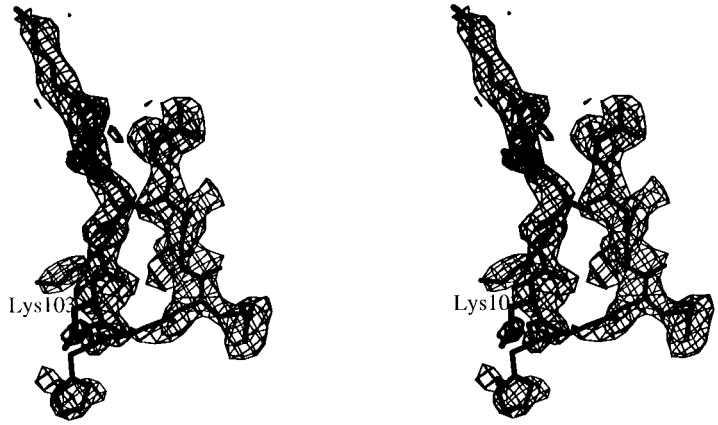

FIGURE 6: Stereodiagram of the $(2F_o - F_c)\alpha_{calc}$ electron density in the 102A-108A loop region. The contouring level is 1σ. The $(2F_o - F_c)\alpha_{calc}$ electron density seen above the loop is a water molecule with hydrogen bonds to Lys103O (3.02 Å) and Gly109N (2.92 Å). Lys103 involved in catalysis is labeled. Figures 3 and 8 are generated with the program O, (Jones *et al.*, 1991).

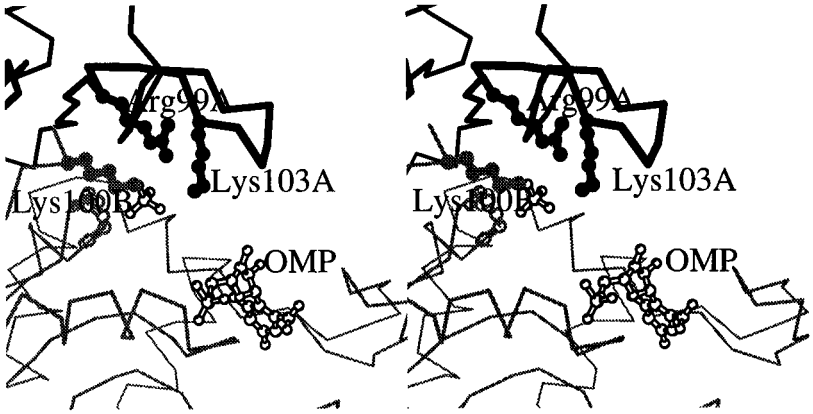

FIGURE 7: Dimer interface of *E. coli* OPRTase with OMP from the *S. typhimurium* structure superimposed. Monomer 1A-213A is in black, while monomer 1B−213B is in grey. Sulfate bound in the pyrophosphate binding site is shown as a ball-and-stick model. Ball-and-stick side chains for Lys103A and Arg99A are in black, while the ball-and-stick side chain for Lys100B is in grey. The grey non filled ball-and-stick main chain atoms are the main chain atoms of Tyr72B and Lys73B.

cal modification after PRPP or pyrophosphate binding, namely, Lys100 and Lys103 (Grubmeyer et al., 1993). This pyrophosphate binding site, like previously described phosphate binding sites, involves a loop from a strand−loop−helix motif, but it additionally includes hydrogen bonds between the sulfate and amino acid residues in segments far away from the strand−loop−helix motif in the primary sequence of the protein. The strand−loop−helix motif responsible for pyrophosphate binding (B3−loop−A3) is a highly conserved motif in the three three-dimensional structures of PRTases, but only in the sulfate-ligated *E. coli* OPRTase has the 71−72 peptide bond been assigned as a cis-peptide. The sulfate binding site in *E. coli* OPRTase corresponds to the regulatory 5′-phosphate binding site for AMP in amido-PRTase (Smith et al., 1994).

The other strand−loop−helix motif involved in phosphate binding in OPRTases, the 5′-phosphate binding sites in the B5-loop-A4 loop, showed no convincing density for sulfate ions.

Sulfate has been found in both monomers in the same orientation although the flexible loop has only been closed and traceable in one monomer. Thus, the binding of sulfate does not lead to a closed flexible loop region, although Lys103 can form a hydrogen bond to the bound sulfate. It rather leads to swapping between an open and a closed active site in the monomer.

A requirement of Mg^{2+} ions has been observed for the OPRTase reaction (Bhatia & Grubmeyer, 1993), in which the Mg^{2+} was found to form a complex with PRPP. A possible role for Mg^{2+} could be to form salt bridges to pyrophosphate/PRPP, thereby shielding their additional charge as compared to sulfate and giving a less flexible binding of the more extended pyrophosphate substrates. There has been no evidence that PRPP can bind to the enzyme in the absence of Mg^{2+}.

Placing OMP at the position where it was found in the *S. typhimurium* enzyme in the sulfate-ligated *E. coli* OPRTase

structure (Figure 7) reveals a distance of 10 Å between OMP ribose C1′ and Lys103N$_\zeta$ in the closed conformation of the flexible loop. In this conformation, ribose C1′ of OMP is fully accessible to solvent. This is also true for most of the flexible loop surface, as no direct amino acid interactions are made with the adjacent monomer. Mutation of Lys103 to alanine or glutamine (Ozturk et al., 1995a) has been shown to decrease k_{cat} 600−1000 fold with virtually no effects on K_m's for PRPP or OMP, whereas no residue near ribose C1′ of OMP in the *S. typhimurium* OPRTase structure has been shown to have any significant impact on catalysis. Bringing the ribose C1′ of OMP in proximity to Lys103N$_\zeta$, in its conformation in the closed flexible loop would require a rotation around a bond in the 5′-phosphate group of OMP. The flexibility in conformation observed for the 5′-phosphate binding site could reflect this site's ability to accommodate a movement of this kind. However, to allow for the movement of OMP into a more favorable conformation, with respect to interactions with Lys103, the flexible loop must be in a solvent exposed, open conformation. The movement of OMP could then be followed by a closure of the flexible loop creating a secondary OMP/orotate binding site in proximity to Lys103 and the bound pyrophosphate. In this way a highly reactive oxocarbonium-like transition state would be protected against solvent and hydrolysis. A possible role for Mg^{2+} could be to form a complex with the ribose part of the OMP molecule. Such a complex would change the OMP hydrogen bonding pattern and could hereby facilitate the movement of OMP into a more favorable conformation with respect to catalysis.

CONCLUSIONS

The pyrophosphate binding site and a closed conformation of the flexible loop involved in OPRTase catalysis have been established. The closed conformation of the flexible loop brings the catalytically active Lys103 within hydrogen-bonding distance of bound sulfate, inhibiting the OPRTase reaction and mimicking the binding of the β-phosphate from pyrophosphate. Comparisons with the previously determined three-dimensional structure of OPRTase in complex with OMP show distances of 10 Å between ribose C1′ and Lys103N$_\zeta$ and of 11 Å between ribose C1′ and sulfate. Furthermore, closure of the flexible loop will only exclude solvent from the surroundings of OMP C1′ if this molecule is moved to a position closer to the position of Lys103 in its closed conformation. If catalysis is to proceed through a highly active transition state as proposed (Goitein et al., 1978), then catalysis must involve large conformational changes to protect the transition state against water. The conformational changes needed will not only concern the flexible loop, but also OMP/orotate. Structures of OPRTase co-crystallized with a transition state analog, with orotate and sulfate, or with OMP, Mg^{2+}, and sulfate might confirm the existence of a secondary orotate/OMP binding site.

The conformation of the flexible loop of *E. coli* OPRTase with bound sulfate is asymmetric. One monomer has the loop in a closed, less flexible conformation, while the other monomer has the loop in an open and highly flexible conformation.

ACKNOWLEDGMENT

We want to thank Derya Ozturk and Charles Grubmeyer for communicating their results on mutant OPRTases prior to publication.

NOTE ADDED IN PROOF

In the complex of *S. typhimurium* OPRTase, orotate, and PRPP recently published by Scapin et al. (1995) the PRPP is bound in a position that is closer to the conserved active site lysine of the flexible loop than the OMP in the previously published structure (Scapin et al., 1994).

REFERENCES

Aghajari, N., Jensen, K. F., & Gajhede, M. (1994) *J. Mol. Biol. 241*, 292−294.

Bhatia, M. B., & Grubmeyer, C. (1993) *Arch. Biochem. Biophys. 303*, 321−325.

Bhatia, M. B., Vinitsky, A., & Grubmeyer, C. (1990) *Biochemistry 29*, 10480−10487.

Brünger, A. T. (1992) *X-PLOR version 3.1. A system for x-ray crystallography and NMR* Yale University Press, New Haven, CT.

Brünger, A. T., Kuriyan, J., & Karplus, M. (1987) *Science 235*, 458−460.

Collaborative Computer Project, Number 4 (1994) *Acta Crystallogr. D50*, 760−763.

Eads, J. C., Scapin, G., Xu, Y., Grubmeyer, C., & Sacchettini, J. C. (1994) *Cell 78*, 325−334.

Goitein, R. K., Chelsky, D., & Parsons, S. (1978) *J. Mol. Biol. 253*, 2963−2971.

Grubmeyer, C., Segura, E., & Dorfman, R. (1993) *J. Biol. Chem. 268*, 20299−20304.

Hershey, H. V. & Taylor, M. (1986) *Gene 43*, 287−293.

Hove-Jensen, B., Harlow, K. W., King, C. J., & Switzer, R. L. (1986) *J. Biol. Chem. 261*, 6765−6771.

Jensen, K. F. (1983) in *Metabolism of Nucleotides, Nucleosides and Nucleobases in Microorganisms* (Munch-Petersen, A., Ed.) pp 1−25, Academic Press, London.

Jensen, K. F., Andersen, J. T., & Poulsen, P. (1992) *J. Biol. Chem.* 267, 17147−17152.

Johnson, G. G., Eisenberg, L. R., & Migeon, B. R. (1979) *Science 203*, 174−176.

Jones, T. A., Zou, J.-Y., Cowan, S. W., & Kjeldgaard, M. (1991) *Acta Crystallogr. A47*, 110−119.

Kabsch, W., & Sander, C. (1983) *Biopolymers 22*, 2577−2637.

Kraulis, P. J. (1991) *J. Appl. Crystallogr. 24*, 946−950.

Laskowski, R. A., MacArthur, M. W., Moss, S. D., & Thornton, J. M. (1993) *J. Appl. Crystallogr. 26*, 283−291.

Musick, D. L. (1981) *Crit. Rev. Biochem. 11*, 1−34.

Navaza, J. (1994) *Acta Crystallogr. A50*, 157−163.

Otwinowski, Z. (1993) *Proceedings of the CCP4 Study Weekend: Data Collection and Processing*, SERC Daresbury Laboratory, England, pp 56−62.

Ozturk, D. H., Dorfman, R. H., Scapin, G., Sacchettini, J. C., & Grubmeyer, C. (1995a) *Biochemistry 34*, 10755−10763.

Ozturk, D. H., Dorfman, R. H., Scapin, G., Sacchettini, J. C., & Grubmeyer, C. (1995b) *Biochemistry 34*, 10764−10770.

Poulsen, P., Jensen, K. F., Valentin-Hansen, P., Carlsson, P., & Lundberg, L. G. (1983) *Eur. J. Biochem. 135*, 223−229.

Richardson, J. S. (1981) *Adv. Protein Chem. 34*, 167−339.

Scapin, G., Grubmeyer, C., & Sacchettini, J. C. (1994) *Biochemistry 33*, 1287−1294.

Schapin, G., Ozturk, D. H., Grubmeyer, C., & Sacchettini, J. C. (1995) *Biochemistry* 34, 10744−10754.

Schulz, G. E. (1992) *Curr. Opin. Struc. Biol. 2*, 61−67.

Smith, J. L., Zaluzec, E. J., Wery, J.-P., Niu, L., Switzer, R. L., Zalkin, H., & Satow, Y. (1994) *Science 264*, 1427−1433.

Strauss, M., Behlke, J., Ampers, F., & Goerl, M. (1978) *Eur. J. Biochem. 90*, 89−97.

Walker, J. E., Saraste, M., Runswick, M. J., & Gay, N. J (1982) *EMBO J. 1*, 945−951.

BI952226Y